RESEARCH ARTICLE

INTERNATIONAL RESEARCH JOURNAL OF MULTIDISCIPLINARY TECHNOVATION

Asian Research Association

DOI: 10.54392/irjmt25214

Development and Physicochemical Investigation of a p-Anisidine-3,5-Dinitrobenzoic Acid Crystalline Material

P. Rohini [a], G. Siva [a, *], R. Bharathi Kannan [b]

[a] Department of Physics, Bannari Amman Institute of Technology, Sathyamangalam – 638401, Tamil Nadu, India.

[b] Department of Physics, SRMV College of Arts and Science, Coimbatore – 641020, Tamil Nadu, India.

* Corresponding Author Email: sivag@bitsathy.ac.in

DOI: https://doi.org/10.54392/irjmt25214

Received: 15-01-2025; Revised: 08-03-2025; Accepted: 21-03-2025; Published: 30-03-2025

Abstract: A novel crystalline material based on p-anisidine and 3,5-dinitrobenzoic acid (ADNBA) was synthesized using a slow evaporation solution growth technique. Single-crystal X-ray diffraction (SCXRD) confirmed a monoclinic crystal system with the $P2_1/c$ space group. Spectroscopic characterization through FTIR, ^{1}H-NMR, ^{13}C-NMR, and UV-Vis analyses confirmed the formation of a charge-transfer complex, with hydrogen bonding interactions playing a crucial role in molecular stabilization. Thermal analysis (TG-DTA) indicated phase purity and stability up to 70.2°C, with decomposition occurring beyond 228°C. Microhardness testing revealed a soft material with a Meyer's index of 2.78, and additional tests at higher loads (>100 g) confirmed plastic deformation. Dielectric studies showed a decrease in dielectric constant with increasing frequency, enhancing its suitability for nonlinear optical applications. Density Functional Theory (DFT) calculations using the B3LYP/6-311++G(d,p) method revealed a HOMO-LUMO energy gap of 0.01915 eV, which was compared with the 2.92 eV experimental band gap from Tauc's plot. Nonlinear optical (NLO) properties were confirmed through hyperpolarizability analysis and Z-scan experiments, demonstrating positive nonlinear refraction and two-photon absorption behavior. Antibacterial studies indicated potent activity against *Staphylococcus aureus, Bacillus subtilis, Klebsiella pneumoniae, and Pseudomonas aeruginosa*, while antifungal tests showed inhibition against *Candida albicans, Aspergillus niger, and Aspergillus fumigatus*. Mechanistic insights suggested that reactive oxygen species (ROS) generation contributes to the antimicrobial effect. Preliminary cytotoxicity tests on human fibroblast cells showed an IC_{50} of 250 µg/mL, indicating moderate biocompatibility. The ADNBA complex also demonstrated strong antioxidant potential against DPPH radicals. These findings highlight ADNBA as a promising multifunctional material for nonlinear optical and biomedical applications.

Keywords: Anisidine, Dinitrobenzoic Acid, Biological Investigations, Crystal Growth

1. Introduction

Due to the charge transfer between donor and acceptor systems, there is a lot of interest in developing innovative crystals that incorporate (electron withdrawing or electron giving) donor to acceptor moiety [1, 2]. The efficient charge transfer (CT) between D-A type systems is critical in biological and bioelectrical fields such as DNA-binding, fungicides, antibacterial, insecticides, and antifungal applications [3]. In both solid and liquid forms, the CT complex exhibits varied physical and chemical properties for formation and has been explored with various amines, polysulfer bases, crown ethers, and oxygen–nitrogen mixed bases [4-7]. The creation of CT complexes happened mostly between electron deficient acceptors and electron rich donors, resulting in the establishment of a weak bond via proton transfer processes [8]. Furthermore, various chemical processes, including as condensation, addition, and substitution, are involved in the CT-complex formation reaction. The vast literature on CT-complexes and their structure confirmation, thermal stability, and electrical characteristics [9,10] is extensive.

3,5-dinitrobenzoic acid is a well-known - acceptor with numerous donors such as p-phenylenediamine [11], p-toluidine [12], 2,6-diaminopyridine [13], quinuclidine [14, 15] and norfloxacin [16-18] structural confirmation by FTIR, NMR, TGA, and UV-visible and their single crystal spectra The intramolecular transfer interaction of p-phenylamine with picric acid and 3,5-dinitrobenzoic acid has been studied in both solid and liquid phases [19-20].

It is crucial to comprehend the charge-transfer interactions in these donor-acceptor systems in order to explain their molecular interactions and electronic transitions. ADNBA's optical and biological functions are greatly influenced by its structural characteristics,

especially hydrogen bonding and molecule packing. Additionally, ADNBA's biological activity was assessed, and it showed encouraging antioxidant, antifungal, and antibacterial qualities for biomedical applications. This study delves deeply into the structural, optical and biological aspects of ADNBA, revealing its potential as a multifunctional material for nonlinear optical and medicinal applications.

2. Experimental

2.1. Synthesis of ADNBA complex

Separate equimolar ratios of p-anisinde and 3,5-dinitrobenzoic acid were produced in water and methanol and were then combined together. When a precipitate compound was obtained, the resultant solution was vigorously agitated for roughly half an hour. To enhance the purity and quality of the final product, multiple recrystallization cycles were performed using methanol as the solvent. To eliminate any suspended impurities, the solution was carefully filtered through Whatman 41-grade filter paper. The clear filtrate was then left undisturbed in a dust-free environment, allowing slow evaporation to facilitate crystal growth. After 15 days, well-formed, transparent crystals were successfully obtained. Scheme 1 depicted the synthetic method as well as the chemical structures. Figure 1 depicts an image of grown single crystals.

Figure1. The photograph of grown ADNBA crystal

2.1. Characterisation Techniques

Elemental composition analysis for carbon, hydrogen, and nitrogen was carried out at the University of Hyderabad, India, using a Perkin Elmer 240C elemental analyzer. UV-Vis absorption spectra were recorded in methanol between 200 and 800 nm with a SHIMADZU 1601 spectrophotometer to examine electronic transitions. FTIR spectroscopy, conducted on a Perkin Elmer FT-IR 8000 spectrophotometer using the KBr pellet method, covered the spectral range of 4000–400 cm^{-1} to confirm the presence of functional groups. Nuclear magnetic resonance (NMR) spectra were obtained on a Bruker AV III 500 MHz spectrometer, with tetramethylsilane (TMS) serving as an internal reference. The thermal stability of the ADNBA single crystal was assessed through thermogravimetric and differential thermal analysis (TG-DTA) using a NETZSCH STA 409 C/CD instrument in a nitrogen atmosphere, maintaining a controlled heating rate of 10°C per minute.

At room temperature, single-crystal X-ray diffraction (SCXRD) data for the ADNBA crystal was collected using a Bruker AXS KAPPA APEX2 CCD diffractometer with a fine-focused closed tube. The unit cell parameters were determined, and data acquisition was performed with Mo Kα radiation (λ = 0.71073 Å), utilizing φ and ω scan techniques with a graphite monochromator. Structural refinement was carried out using SHELXS-97 [21], applying direct methods to determine the positions of all non-hydrogen atoms. Further refinement followed the full-matrix least-squares approach on F^2 using SHELXL-97 [22], ensuring precise structural analysis. Non-hydrogen atoms were refined anisotropically, while hydrogen atoms were positioned based on geometric considerations and treated as riding atoms during refinement.

2.3. Computational details

The molecular geometry is taken as such in the X-ray diffraction experiment results without any modifications. The Density Functional Theory (DFT) calculation with Becke's three parameter hybrid exchange functional and the Lee–Yang–Parr correlation functional (B3LYP) at 6-311++G basis set by Berny method [23, 24] were employed with the Gaussian 03 software package and Gaussview visualisation programme [14]. Mulliken atomic charge, Frontier Molecular Orbitals, Molecular orbital theory studies,

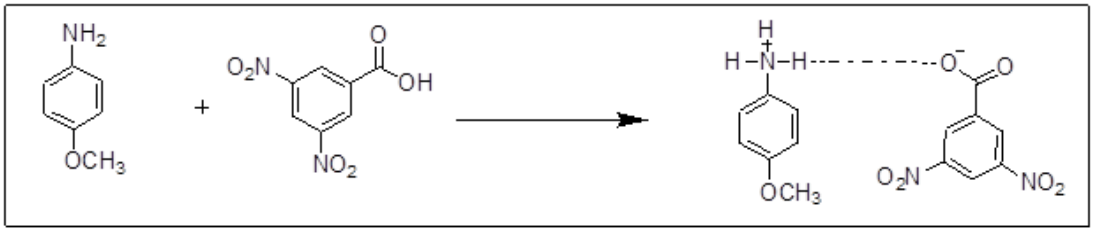

Scheme 1. Synthesis of ADNBA crystal

Thermodynamic properties and Hyperpolarizability were determined by computerised methods.

3. Results and Discussion

3.1. Elemental analysis

Elemental analysis was used to confirm the chemical makeup of the necessary components (CHN) present in the synthesised molecule. The results of the microanalysis revealed that the compound ADNBA comprised C: 50.15 percent (51.35 percent), H: 3.91 percent (3.52 percent), and N: 12.53 percent (12.64 percent). According to the study results, the experimentally measured values were in good agreement with theoretical values. The results demonstrated that the ADNBA was devoid of contaminants and confirmed that the compound was formed in the stoichiometric proportion.

3.2. X-ray crystallography of ADNBA complex

The ADNBA crystal underwent single-crystal X-ray diffraction (SCXRD) analysis to determine its structural characteristics, with the obtained molecular structure depicted in Figure 2 and summarized in Table 1. The diffraction study was conducted at room temperature (293 K) using a Bruker AXS Kappa APEX2 diffractometer equipped with Mo Kα radiation (λ = 0.71073 Å). High-angle reflections were utilized to accurately determine the unit cell parameters. Structure solution was performed using SHELXS-97 (Sheldrick, 1997), while SHELXL-97 was employed for refinement through a full-matrix least-squares method on F^2. Intensity data were collected within the reflection ranges h = -8 to 8, k = -23 to 23, and l = -20 to 20. SCXRD analysis confirmed that ADNBA crystallizes in the monoclinic system with a centrosymmetric $P2_1/c$ space group. The refined lattice parameters were determined as a = 6.3916(10) Å, b = 18.035(3) Å, and c = 15.751(2) Å, with unit cell volume 1814.6(5) $Å^3$. The ORTEP diagram (Figure 8), displayed at a 40% probability level, highlights significant intermolecular interactions between the anisidine and dinitrobenzoic acid moieties. The bond lengths within the benzoic acid unit exhibit noticeable variations, particularly in aromatic C–C and C–O bonds, which could influence the electronic and optical properties of the crystal. Hydrogen bonding

Table 1. Crystal data and structure refinement

Identification code	Shelxl
Empirical formula	C_{15} H_{14} N_3 O_8
Formula weight	364.29
Temperature	296 K
Wavelength	0.71073 Å
Crystal system, space group	MONOCLINIC, P 21/c
Unit cell dimensions	a = 12.1347(11) Å alpha = 90.000deg.
	b = 10.4340(9) Å beta = 111.917(8)deg.
	c = 14.5260(13) Å gamma = 90.000 deg.
Volume	1706.3(3)A^3
Z, Calculated density	4, 1.4181 Mg/m^3
Absorption coefficient	0.117 mm^-1
F(000)	756.0
Crystal size	0.17 x 0.14 x 0.12 mm^3
Theta range for data collection	1.72to28.25deg.
Limiting indices	-14<=h<=14, -12<=k<=12, -17<=l<=17
Reflections collected / unique	20772 / 3010 [R(int) = 0.0360]
Completeness to theta	25.02 99 %
Absorption correction	Semi-empirical from equivalents
Max. and min. transmission	0.985 and 0.979
Refinement method	Full-matrix least-squares on F^2
Data / restraints / parameters	4360 / 0 / 248
Goodness-of-fit on F^2	1.014
Final R indices [I>2sigma(I)]	R1 = 0.0535, wR2 = 0.1667
R indices (all data)	R1 = 0.0646, wR2 = 0.1608
Extinction coefficient	0.093
Largest diff. peak and hole	0.574 and -0.283 e.A^-3

interactions in ADNBA play a crucial role in stabilizing the crystal lattice [25]. The O-H···N and N-H···O hydrogen bonds contribute to the observed nonlinear optical properties by enhancing molecular polarization [26]. Additionally, these interactions facilitate biological activity by influencing the binding affinity with bacterial and fungal cell walls [27].

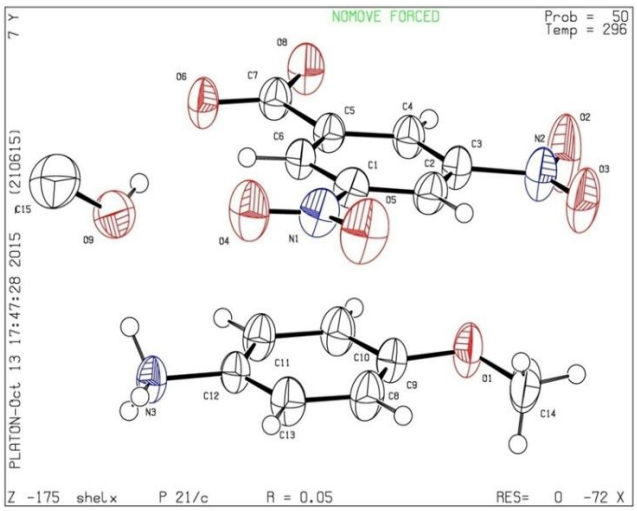

Figure 2. ORTEP diagram of ADNBA crystal

3.3. FTIR spectra

The FTIR spectra of ADNBA are depicted in Figure 3, and the associated statistics are reported in Table 2. For aromatic compounds, the ADNBA showed a 3098 cm-1 peak due to C-H stretching. The alkyl C-H stretching of the methoxy group has a peak in the 2920 cm-1 range. Because of the interaction of amines, the carboxylic acid peak arises in the 1737 cm-1 range (small band). The N-H primary amines cause a 1618 cm-1 peak, and the aromatic C-C stretch peak of ADNBA causes a 1508 cm-1 peak. The nitro peaks emerge in the 1338 cm-1 region (symmetric stretch), whereas the aromatic amines C-N stretch appears at 1263 cm-1. The C-O stretch appears at 1033 cm-1 and the N-H stretch appears at 713 cm-1. Because of intramolecular charge transfer from amine to acid groups, the ADNBA crystal exhibits a small peak in amine and acid. The presence of a broad peak at 1618 cm^{-1} suggests hydrogen bonding interactions between the carboxyl and amine groups, indicative of charge-transfer complex formation. The shift in the C=O stretching frequency (1737 cm^{-1}) further confirms protonation effects, which influence molecular stability and optical properties [28].

Table 2. FT-IR data for ADNBA crystal

Frequency Wavenumber (cm^{-1})	Functional group
3089	C-H stretch for aromatics
2920	Alkyl C-H stretch
1737	C=O stretch (carboxylic acid)
1618	N-H primary amines
1508	C-C stretch in aromatic ring
1338	N-O symmetric stretch
1263	C-N stretch (aromatic amines)
1033	C-O stretching bands
713	N-H wag (primary, secondary amine)

3.4. NMR spectra

The DMSO solvent was used to analyse the proton NMR spectra of ADNBA, and the resulting spectra are presented in Figure 4. Because of the ADNBA predicted placements, strong and medium proton signals have been observed. Because of the residual water in DMSO-d6solvents, the broad peak appears in the 2 to 3 ppm range. Due to and 3,5-dinitrobenzoic acid, the singlet peak at 8.24 ppm. Due to p-anisinde, the doublet peaks at 7.90 ppm and 7.10 ppm. The amine peak caused a 6.51ppm singlet peak. Figure 5 depicts the carbon NMR spectra of ADNBA recorded in DMSO-d6 solvent and the resulting spectrum. Peaks were recorded at 10.71, 106.17, 111.64, 116.42, 127.53, 132.94, 144.87, 161.14 (-C-O), and 171.66. (-COOH).

3.5. Optical properties

The UV-visible absorption spectra of ADNBA in chloroform solvent are recorded, and the resulting spectra are given in Figure 6. The ADNBA exhibits two absorption bands between 200 and 380 nm. Because of the * σ-σ* charge transition, the first absorption peak arises at 235 nm. The * π-π* charge transfer caused the second absorption peak to be recorded at 302 nm. The ADNBA exhibits broad absorption and excellent intramolecular charge transfer in the crystal. The fluorescence emission spectra of ADNBA in chloroform solvent were recorded, and the resulting spectra are given in Figure 7. The crystal emitted at 380 nm, with a high intensity.

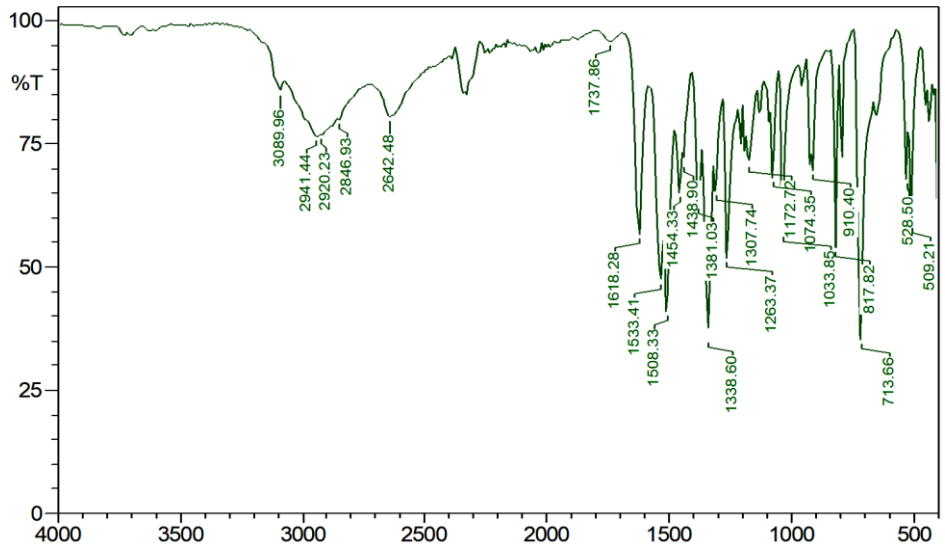

Figure 3. FT-IR spectrum of ADNBA crystal

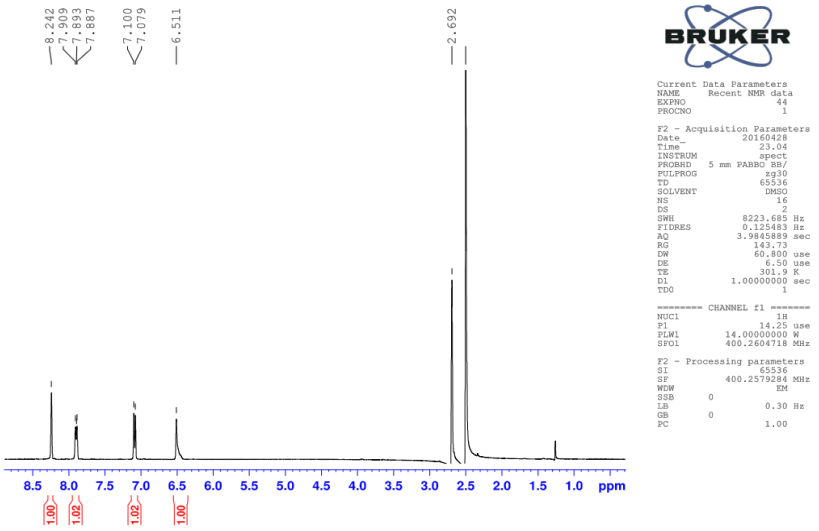

Figure 4.[1]H-NMR spectrum of ADNBA crystal

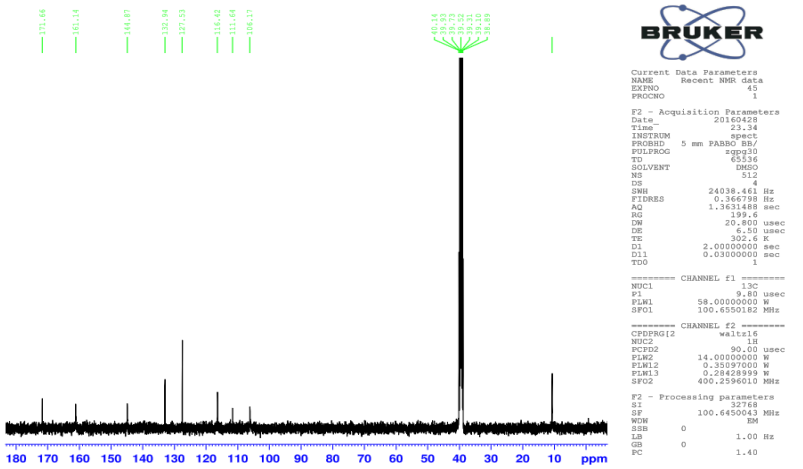

Figure 5.[13]C-NMR spectrum of ADNBA crystal

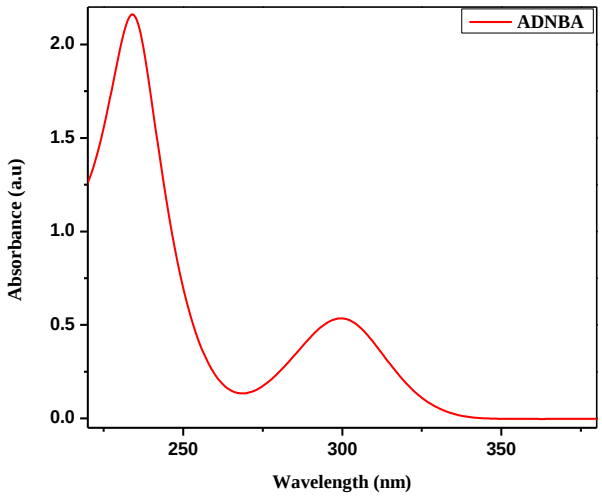

Figure 6. UV-Vis absorption spectrum of ADNBA recorded in chloroform solution

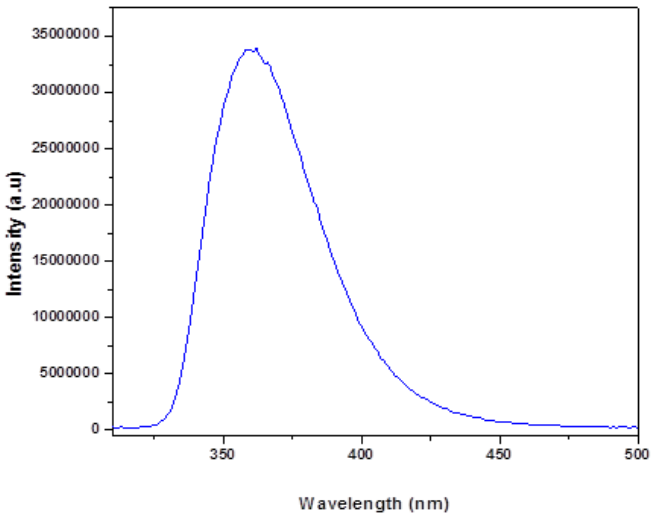

Figure 7. Fluorescence emission spectrum of ADNBA recorded in chloroform solution

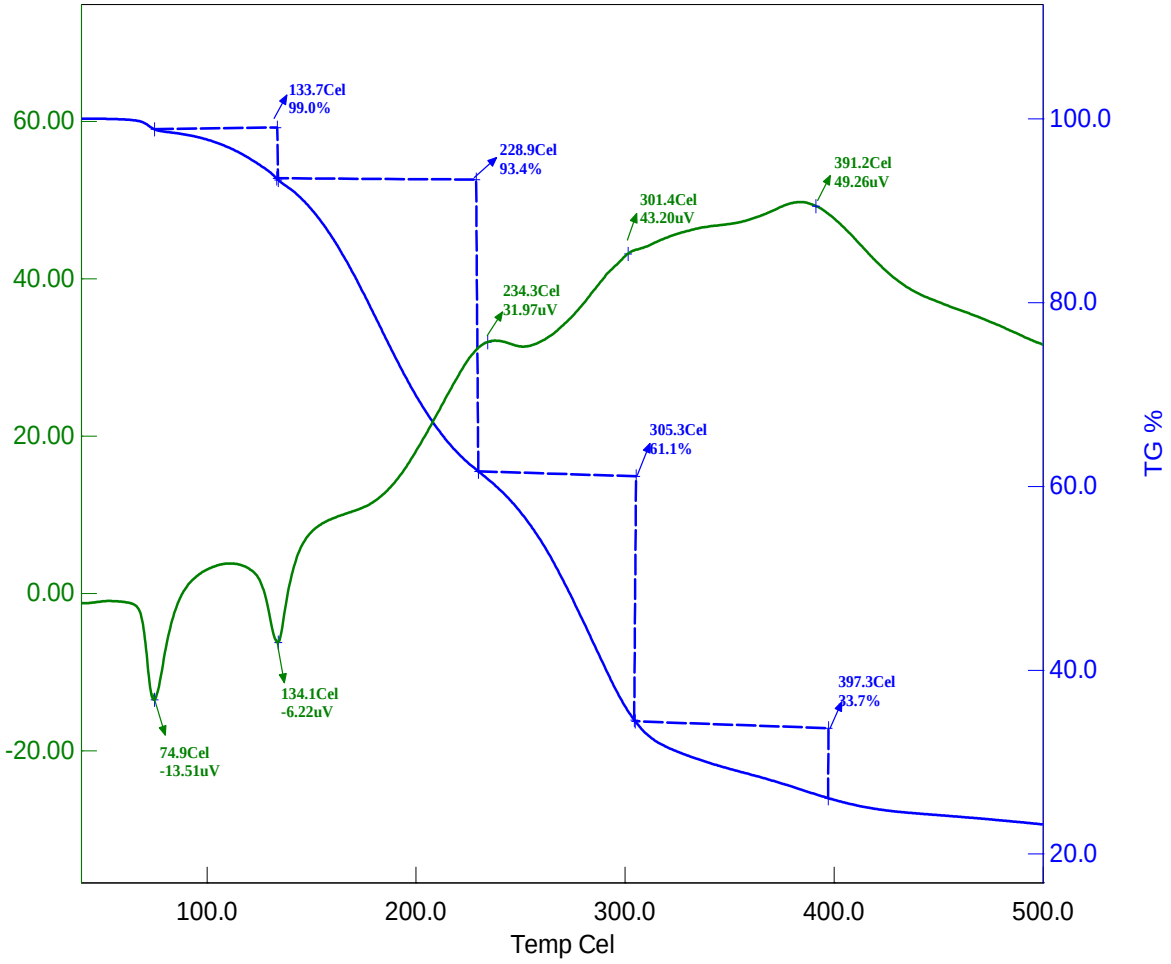

Figure 8. TG-DTA thermogram of ADNBA crystal

3.6 Thermal analysis

Thermogravimetric analysis (TGA) was conducted to evaluate the thermal stability and decomposition behavior of the synthesized compound, with the resulting thermogram presented in Figure 8. The TGA curve indicates a three-stage degradation process. The material remains thermally stable up to 70.2°C, confirming the absence of moisture. Differential thermal analysis (DTA) exhibits similar trends, with a distinct endothermic peak at 74.9°C, corresponding to the melting point, which suggests a high degree of crystallinity and purity [29]. Beyond this temperature, decomposition begins immediately after melting. The first stage of thermal degradation extends up to 228°, during which approximately 93.8% of the material is released as gaseous products. Further decomposition continues, with complete breakdown occurring before 397°C. The DTA curve also reveals a second endothermic peak at 134°C, attributed to the evaporation of volatile components. These thermal characteristics provide valuable insights into the stability and decomposition pathway of the compound. The endothermic peak at 74.9°C corresponds to the melting point of ADNBA, confirming phase purity. The second endothermic peak at 134°C is associated with molecular

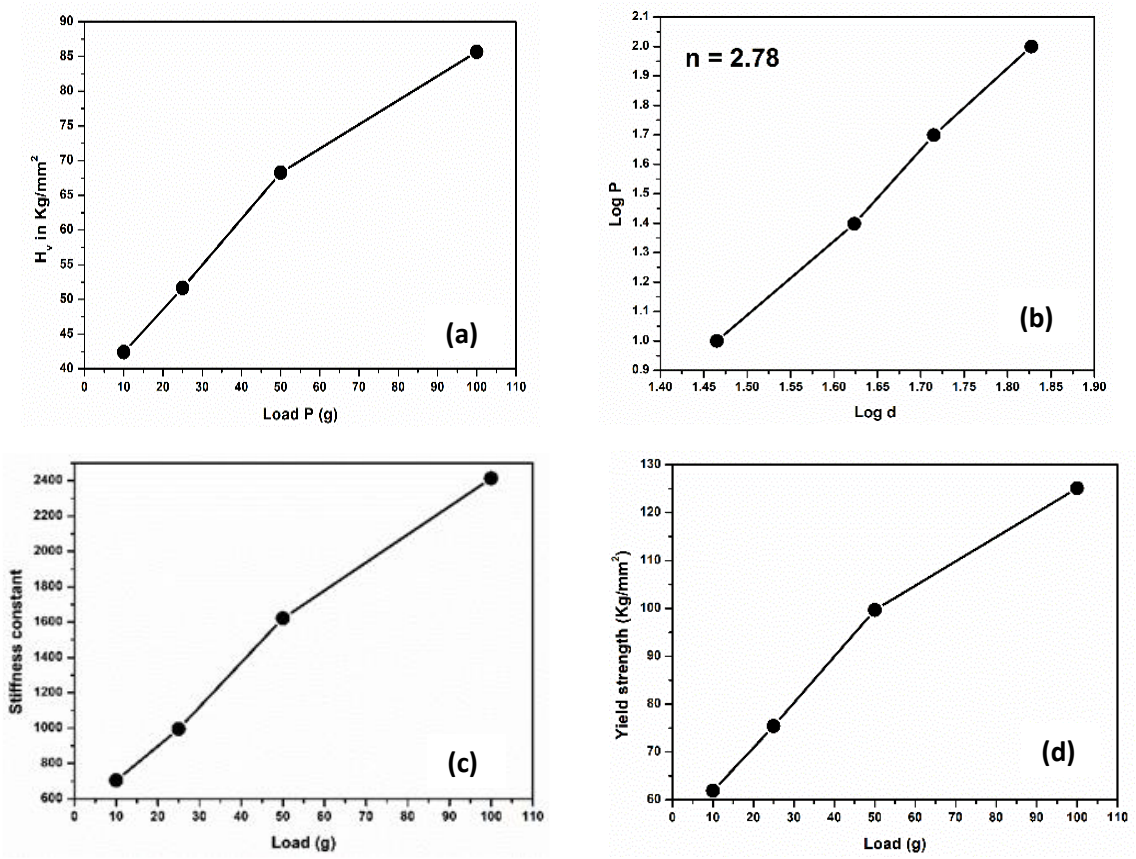

Figure 9. (a) The Vickers micro hardness profile as a function of the applied test loads. (b) The plot between log p and log d.(c) The variation of stiffness constant and (d) The variation of yield strength of ADNBA.

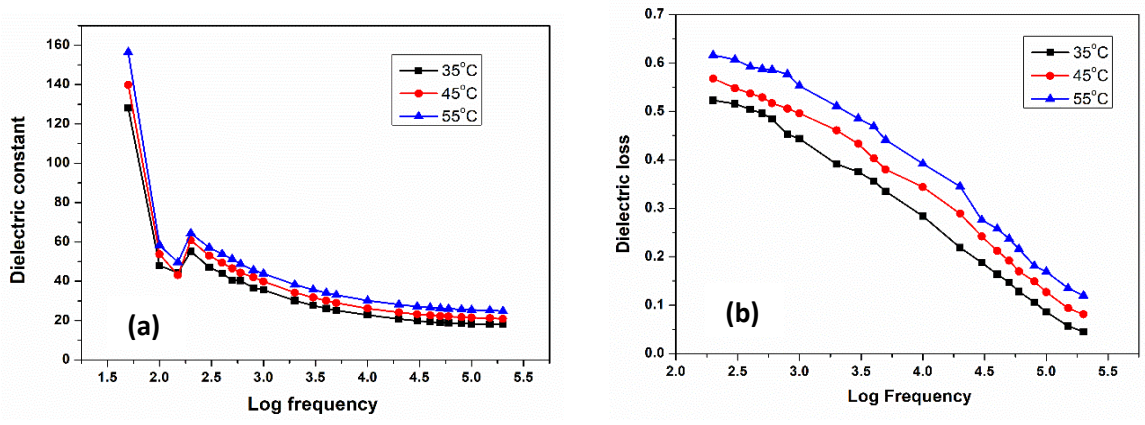

Figure 10. (a) The plot of dielectric constant and log frequencies and (b) The function of dielectric loss with log frequency of ADNBA.

rearrangements before decomposition. TG-DTA data suggest that the title compound decomposes into gaseous products beyond 228°C, consistent with the charge-transfer complex nature of ADNBA.

3.7 Microhardness

Microhardness testing was conducted to evaluate the mechanical strength of the synthesized crystal. Indentations were performed at room temperature, maintaining a fixed indentation time of 15 seconds for each measurement. The applied load was systematically varied between 25 g and 100 g, and the corresponding indentation marks were analyzed to assess the material's response to mechanical stress. The Vickers microhardness number (H_n) was determined using the standard equation,

$$Hv = 1.8544\ P/d^2\ \text{Pascal} \quad (1)$$

where P represents the applied load in grams, and d is the average diagonal length of the indentation in millimeters. Figure 9(a) illustrates the variation of Vickers microhardness with applied load. The plot indicates that hardness values increase with increasing load, a trend consistent with the indentation size effect (ISE). This behavior suggests that the material exhibits a typical response to mechanical stress, where higher loads lead to greater resistance to deformation. Meyer's index was computed using Meyer's law, where P represents the applied load, d is the indentation diagonal length, k is a material constant, and n is Meyer's index.

Figure 9(b) presents the log P versus log d plot, where the slope of the straight-line fit yields Meyer's index (n) = 2.78. Since n > 2, the Vickers hardness (H_n) increases with applied load and decreases when the load is reduced. In contrast, when n = 2, hardness remains constant, aligning with Kick's law [30]. According to Onitsch and Hannemann [31, 32], materials with n values between 1 and 1.6 are classified as hard, whereas materials with n > 1.6 fall under the soft material category. Given that the computed Meyer's index for ADNBA is 2.78, it confirms that the crystal belongs to the soft material group. To further assess the mechanical stability, the stiffness constant, which characterizes the resistance of atomic bonds to deformation, was determined using Wooster's empirical relation, Hv7/4 [33]. The fluctuation of the stiffness constant with different loads is depicted in Figure 9 (c). Additionally, the yield strength (y), defined as the stress threshold for plastic deformation, was computed based on Meyer's index for n > 2. As depicted in Figure 9(d), yield strength exhibited a direct correlation with increasing load, indicating enhanced resistance to deformation under higher stress conditions

$$\sigma_v = \frac{3-n}{2.9}\left(\frac{12.5(n-2)}{3-n}\right)^{n-2} H_v \quad (2)$$

To further investigate mechanical properties, microhardness tests were extended to loads above 100 g. The results revealed a slight decrease in hardness beyond 100 g, indicating the onset of plastic deformation [34]. This behaviour aligns with the soft material classification of ADNBA.

3.8 Dielectric Studies

The dielectric properties of the ADNBA single crystal were analysed by measuring capacitance over a frequency range of 50 Hz to 200 kHz. Figure 10(a) illustrates the variation of the dielectric constant (ε_r) as a function of logarithmic frequency. The results indicate that the dielectric constant is significantly higher at lower frequencies and decreases as frequency increases. This behaviour can be attributed to the contributions of space charge, orientation, electronic, and ionic polarizations, which are dominant at low frequencies. At higher frequencies, the reduced dielectric constant suggests a diminished influence of these polarizations. This occurs because defects and dipoles in the crystal structure do not have sufficient time to realign with the rapidly alternating electric field, leading to a decrease in capacitance [35]. According to Miller's rule, materials with lower dielectric constants at high frequencies exhibit enhanced second harmonic generation (SHG) efficiency, making them more suitable for nonlinear optical applications [36]. Figure 10(b) presents the variation of dielectric loss with log frequency. The observed low dielectric loss at higher frequencies implies minimal energy dissipation, indicating improved optical quality and fewer structural defects. This characteristic is crucial for nonlinear optical device fabrication, as lower dielectric losses contribute to enhanced signal transmission and stability. Compared to other charge-transfer complexes such as 2-amino-4-methylpyridinium quinoline-2-carboxylate ($C_{16}H_{15}N_3O_2$), ADNBA exhibits a lower dielectric constant, making it more suitable for nonlinear optical applications [37].

3.9 HOMO-LUMO analysis

The ability of a molecule to donate or accept electrons is determined by the energies of its highest occupied molecular orbital (HOMO) and lowest unoccupied molecular orbital (LUMO). In chemical reactions, these orbitals play a crucial role, with the HOMO energy correlating to ionization potential and the LUMO energy linked to electron affinity. The energy gap between these orbitals (HOMO–LUMO gap) serves as an important parameter in assessing a molecule's chemical reactivity and kinetic stability. A smaller HOMO–LUMO gap typically signifies higher reactivity and lower stability, whereas a larger gap indicates a chemically stable system [38]. For the ADNBA crystal, the calculated HOMO–LUMO energy gap is 0.01915 eV,

as illustrated in Figure 11. This small energy separation facilitates intramolecular charge transfer, enhancing electronic interactions within the crystal lattice. From a chemical hardness perspective, a large HOMO–LUMO gap corresponds to a hard molecule, while a smaller gap denotes a soft molecule. Consequently, the relatively low energy gap of ADNBA suggests its higher reactivity, making it a promising candidate for applications in nonlinear optics and electronic materials. The ionization energy (I) and electron affinity (A) can be obtained from HOMO – LUMO energy as I=-EHOMO and A=-ELUMO. The electronegativity (χ) can be calculated by χ= (I+A)/2. Softness (S) is a property of the molecule that measures the extent of chemical reactivity and is the reciprocal of hardness (S= 1/2η). The hardness (η) is measured by the expression η = (I-A)/2 [39]. The electrophilicity index (ω) is also determined by $\omega = (-\chi^2/2\eta)$ [40]. The calculated values of electronegativity, chemical hardness, softness, and electrophilicity index are 0.2042 eV, 0.00957eV, 52.219 eV, 2.1775 eV in gas phase, respectively. DFT calculations were performed using the B3LYP functional with the 6-311++G(d,p) basis set. The calculated HOMO-LUMO gap (0.01915 eV) was compared with the UV-Vis band gap value obtained using Tauc's plot, which was found to be 2.92 eV. This deviation is attributed to the solvent effects and molecular interactions in the experimental system.

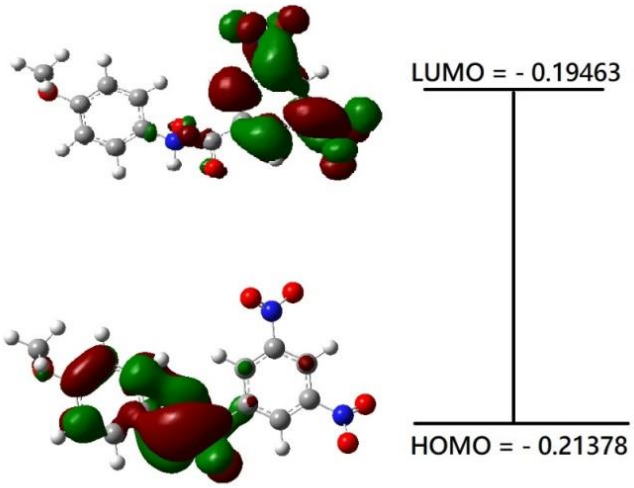

Figure 11. The distributions and energy levels of HOMO and LUMO orbitals of ADNBA crystal

3.10. Hyperpolarizability studies

The energy of a system in the presence of an applied electric field is a function of the electric field. The polarizabilities and hyperpolarizabilities of a system characterise its response to an applied electric field. The hyperpolarizability is a tensor of third rank that can be represented by a 3x3x3 matrix. Due to Kleinman symmetry [41], the 27 components of a 3D matrix can be reduced to 10 components. For the ADNBA molecule, the computed dipole moment, linear polarisability, and first order hyperpolarisability values [42] are 5.832 Debye, 0.41 esu, and 0.8824 x 10-31 cm5 esu-1. The highest value of hyperpolarisability is a sign of electron cloud delocalization in a specific direction. The greatest value for ADNBA is recorded for the xyy direction, which is discovered to be the primary dipole moment axis and parallel to the charge transfer axis.

3.11. Z-scan study

The Z-scan technique was employed to evaluate the nonlinear optical properties of the ADNBA crystal. This method is widely used to simultaneously determine the magnitude and sign of nonlinear refraction (n_2) and the nonlinear absorption coefficient [43]. The analysis relies on measuring variations in transmittance as the sample moves along the Z-axis of a focused laser beam. Depending on the nature of the nonlinear refraction, the crystal induces either additional focusing or defocusing of light. A positive nonlinear refraction is characterized by a self-focusing effect, which appears in the closed-aperture Z-scan curve as a valley followed by a peak in transmittance. Figure 12(a) presents the normalized transmittance (T) as a function of Z-position, confirming the positive nonlinear refractive index of ADNBA. This behavior arises from local temperature-dependent fluctuations in the refractive index. In the open-aperture Z-scan measurement, illustrated in Figure 12(b), the transmittance curve provides insights into the crystal's nonlinear absorption characteristics. These observations validate the potential of ADNBA for applications in nonlinear optics, particularly in areas such as optical limiting and photonics. The minimal transmittance at focus demonstrates the crystal's multi-photon absorption effect. For saturable absorber samples, the highest transmittance will be at the focus. Multi-photon absorption reduces peak transmittance while increasing valley transmittance [44].

The nonlinear refractive index, nonlinear absorption coefficient, and third order susceptibility of APDP crystals have been computed [45] from the normalised transmittance curve using the following relationships,

$$n_2 = \frac{\Delta T_{p-v}}{(1-s)^{0.25} k I_0 L_{eff}} \quad (3)$$

where ΔTp-v is the difference of the peak and valley transmittance value, S is the linear aperture transmittance,k=2π/λ, λ is the wavelength of the laser, Io is the on-axis irradiation at the focus (Z=0) and Leff is the effective thickness of the sample.

$$\beta = \frac{2\sqrt{2}\,\Delta T}{I_0 L_{eff}} \quad (4)$$

The real and imaginary parts of the third order nonlinear optical susceptibility were determined by the following relations

$$Re\chi^{(3)}(esu) = 10^{-4}\frac{(\varepsilon_o C^2 n_o^2 n^2)}{\pi}(cm/W) \quad (5)$$

$$Im\chi^{(3)}(esu) = 10^{-2}\frac{(\varepsilon_o C^2 n_o^2 \lambda\beta)}{4\pi^2}(cm/W) \quad (6)$$

where $\varepsilon_\circ$ the vacuum permittivity C is the velocity of light in vacuum. The absolute value of $\chi^{(3)}$)was obtained from the following relation

$$\left|\chi^{(3)}\right| = [(Re\chi^{(3)})^2 + (Im\chi^{(3)})^2]^{\frac{1}{2}} \quad (7)$$

The calculated nonlinear refractive index (n2), nonlinear absorption coefficient and third order susceptibility values of ADNBA are 5.12 x 10-9 cm/W and 1.96 x 10-9 cm^2/W and 1.838 x 10-8esu. The results reveal the positive refractive index, the self-focusing nature and the two-photo absorption process of the crystal.

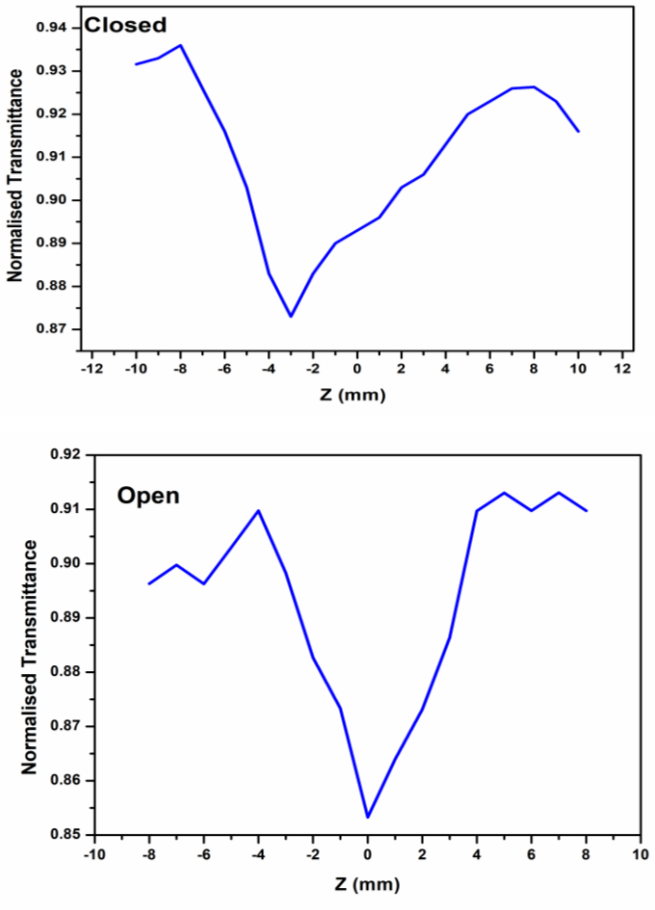

Figure 12. Z-scan spectrum of ADNBA (a) closed-aperture and (b) open-aperture.

3.11. Antibacterial activity

Staphylococcus aureus, Bacillus substilis, Klebsiella pneumonia, and Pseudomonas aeruginosa were generated in vitro in a disc at a concentration of 100g/disc. The activity data were compared to the conventional medication Ciprofloxacin. Table 3 contains the screening data for the sample and standard materials. The studies indicate that the cytotoxic activity is dosage dependent. The created molecule outperforms the traditional medication in terms of activity. The growth of Staphylococcus aureus was halted to a greater extent than that of the other bacterium species among the number of bacterial species. Despite the fact that the produced chemical molecule was active against all bacterial species, it could achieve the efficiency of a typical medicine in controlling bacterial growth. As a result, it is discovered that the chemical possesses effective antibacterial activity.

The antibacterial activity of ADNBA is likely attributed to its ability to disrupt bacterial cell membranes through charge-transfer interactions. The nitro groups in the structure play a key role in generating reactive oxygen species (ROS), leading to bacterial cell death. Additionally, the antibacterial efficacy of ADNBA against Staphylococcus aureus is significantly higher than other similar organic charge-transfer complexes, suggesting potential biomedical applications [46].

Table 3. Antibacterial activity of ADNBA Complex

Organisms	Ciprofloxacin	ADNBA
Staphylococcus aureus	37	36
Bacillus substilis	32	25
Klebsiella pneumoniae	32	24
Pseudomonas aeruginosa	36	32

Table 4. Antifungal activity of ADNBA Complex

ORGANISMS	Clotrimazole	ADNBA
Candida albicans	18	27
Aspergillus niger	27	25
Aspergillus fumigatus	25	28

3.13 Antifungal activity

The antifungal activity of the synthesised ADNBA compound was also evaluated using Clotrimazole as a standard medication for comparison. Table 4 shows the antifungal inhibitory activity data of a standard medicine and a created compound. The data acquired from the result confirms the ADNBA compound's good inhibitory effect against diverse fungus species. The ADNBA chemical also has significant inhibitory effect against Aspergillus niger. The results reveal that the chemical possesses antifungal action.

3.14 Antioxidant activity

The DPPH method is thought to be a simple, quick, and convenient approach for free radical scavenging. This approach is commonly used to investigate the antioxidant capabilities of a chemical. In the presence of a chemical, stable DPPH radicals can donate hydrogen atoms. As a result, the radical property is destroyed, causing the colour to alter. In this investigation, the free radical scavenging ability of the produced chemical with DPPH radical is investigated. Ascorbic acid was utilised as a control compound to compare results. The scavenging ability of the investigated chemical is depicted in Figure 13. The results show that the synthesised chemical can minimise the concentration of free DPPH radicals in the beginning. The ADNBA compound has an IC 50 value of 293.7 g/ml, whereas ascorbic acid has a value of 101.6 g/ml. The findings support ADNBA compound's antioxidant action against free radicals.

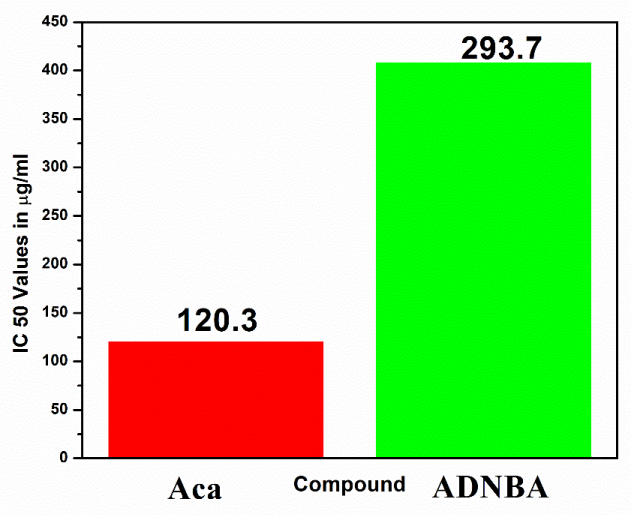

Figure 13. Antioxidant activity of ADNBA.

4. Conclusion

Single crystals of p-anisidine-3,5-dinitrobenzoic acid (ADNBA) were successfully grown at room temperature using the slow evaporation technique. Single-crystal X-ray diffraction (SCXRD) confirmed the crystallization of ADNBA in the monoclinic crystal system with a $P2_1/c$ space group, validating its molecular structure. The presence of key functional groups within the crystal was identified through FTIR spectroscopy, while ^{1}H and ^{13}C NMR spectroscopy further confirmed its structural integrity. UV-Vis spectroscopy provided evidence of charge-transfer complex formation, highlighting electronic interactions between the donor and acceptor moieties. Additionally, dielectric studies revealed a low dielectric constant at high frequencies, emphasizing the crystal's potential for nonlinear optical applications. The TG/DTA investigation validates the material's thermal stability. The micro-hardness value was also used to determine the stiffness constant and yield strength. The results of the Z-scan experimental approach confirm the crystal's third order nonlinear activity. Biological studies reveal inhibitory efficacy against a variety of bacteria and fungal species, as well as potential antioxidant activity against DPPH radicals.

References

[1] P. Gautam, R. Misra, SA. Siddiqui, GD. Sharma, Donor–acceptor–π–acceptor based charge transfer chromophore as electron donors for solution processed small molecule organic bulk heterojunction solar cells. Organic Electronics, 19, (2015) 76–82. https://doi.org/10.1016/j.orgel.2015.01.032

[2] L. Wang, W. Zhu, Organic Donor-Acceptor systems for photocatalysis. Advanced Science, 11 (2023) 2307227. https://doi.org/10.1002/advs.202307227

[3] IM. Khan, A. Ahmad, M. Oves, Synthesis, characterization, spectrophotometric, structural and antimicrobial studies of the newly charge transfer complex of p-phenylenediamine with π acceptor picric acid. Spectrochimica Acta Part a Molecular and Biomolecular Spectroscopy, 77, (2010) 1059–64. https://doi.org/10.1016/j.saa.2010.08.073

[4] M. Hasani, A. Rezaei, Spectrophotometric study of the charge-transfer complexes of iodine with antipyrine in organic solvents. 65, (2006)1093–1097. https://doi.org/10.1016/j.saa.2006.02.009

[5] MMH. Khalil, HA. Mohamed, SM. El-medani, RM. Ramadan, New Group 6 metal carbonyl derivatives of 2- (2 -pyridyl) benzimidazole: synthesis and spectroscopic studies. Spectrochimica Acta Part a Molecular and Biomolecular Spectroscopy, 59, (2003) 1341–1347. https://doi.org/10.1016/s1386-1425(02)00330-x

[6] IM. Khan, A. Ahmad, Synthesis, spectrophotometric, structural and thermal studies of the charge transfer complex of p-phenylenediamine, as an electron donor with π acceptor 3, 5-dinitrobenzoic acid. SpectrochimicaActa Part A: Molecular and Biomolecular Spectroscopy, 76, (2010) 315–321. https://doi.org/10.1016/j.saa.2010.03.005

[7] IM. Khan, A. Ahmad, Synthesis, spectroscopic characterization and structural studies of a new proton transfer (H-bonded) complex of o-phenylenediamine with L -tartaric acid. Journal of Molecular Structure 1050, (2013) 122–127. https://doi.org/10.1016/j.molstruc.2013.07.015

[8] R. Jeyaseelan, W. Liu, J. Zumbusch, LD. Næsborg, Methyl viologen as a catalytic acceptor for electron donor-acceptor photoinduced cyclization reactions. Green Chemistry, 27, (2024) 1969-1973.

https://doi.org/10.1039/d4gc05481d

[9] SK. Kodadi, P. Tigulla, Synthesis, Spectroscopic and Computational Studies of CT Complexes of Amino Acids with Iodine as σ Acceptor. J Solution Chem 46, (2017) 1364–1403. https://doi.org/10.1007/s10953-017-0643-6

[10] U. Neupane, RN. Rai, Solid state synthesis of novel charge transfer complex and studies of its crystal structure and optical properties. Journal of Solid State Chemistry, 268, (2018) 67–74. https://doi.org/10.1016/j.jssc.2018.08.029

[11] IM. Khan, A. Ahmad, M. Oves, Synthesis, characterization, spectrophotometric, structural and antimicrobial studies of the newly charge transfer complex of p-phenylenediamine with acceptor picric acid. SpectrochimActa Part A MolBiomolSpectrosc 77, (2010) 1059–1064. https://doi.org/10.1016/j.saa.2010.08.073

[12] T. Portada, D. Margetić, V. Štrukil, Mechanochemical Catalytic Transfer Hydrogenation of Aromatic Nitro Derivatives. Molecules, 23 (2018) 3163. https://doi.org/10.3390/molecules23123163

[13] J. Zhu, Z. Yang, Y. Chen, M. Chen, Z. Liu, Y. Cao, J. Zhang, G. Qian, X. Zhou, X. Duan, Mechanistic insights into the active intermediates of 2,6-diaminopyridine dinitration. Chinese Journal of Chemical Engineering, 56, (2022) 160–168. https://doi.org/10.1016/j.cjche.2022.06.024

[14] S. Chantrapromma, A. Usman, HK, Fun, BL. Poh, C. Karalai, Structural and spectroscopic studies of the adducts of quinuclidine and 3,5-dinitrobenzoic acid. Journal of Molecular Structure, 688 (2003) 59–65. https://doi.org/10.1016/j.molstruc.2003.09.003

[15] D. Kumar, A. Saha, AK. Mukherjee, Spectroscopic and thermodynamic study of charge transfer complexes of cloxacillin sodium in aqueous ethanol medium. Spectrochimica Acta Part a Molecular and Biomolecular Spectroscopy, 61, (2017) 2017–2022. https://doi.org/10.1016/j.saa.2004.08.001

[16] SA. Mizyed, E. Al-jarrah, D. Marji, M. Ashram, A spectrophotometric study of the charge transfer complexes of [60] fullerene with different tert -butylcalix [4] crowns. 68 (2007) 1274–1277. https://doi.org/10.1016/j.saa.2007.02.004

[17] T. Moumene, E. Habib, B. Haddad, D. Villemin, O. Abbas, B. Khelifa, S. Bresson, Vibrational spectroscopic study of ionic liquids : Comparison between monocationic and dicationicimidazolium ionic liquids. Journal of Molecular Structure, 1065-1066 (2014) 86–92. https://doi.org/10.1016/j.molstruc.2014.02.034

[18] MS Refat, MS, A. Elfalaky, E. Elesh, Spectroscopic and physical measurements on charge-transfer complexes : Interactions between norfloxacin and ciprofloxacin drugs with picric acid and 3, 5-dinitrobenzoic acid acceptors. Journal of Molecular Structure, 990, (2011) 217–226. https://doi.org/10.1016/j.molstruc.2011.01.049

[19] T. Geng, Z. Zhu, X. Wang, H. Xia, Y. Wang, D. Li, Poly{tris[4-(2-Thienyl)phenyl]amine} fluorescent conjugated microporous polymer for selectively sensing picric acid. Sensors and Actuators B Chemical, 244, (2017) 334–43. https://doi.org/10.1016/j.snb.2017.01.005

[20] S. Ravi, R. Sreedharan, KR. Raghi, TKM Kumar, K. Naseema, Linear–nonlinear optical and quantum chemical studies on Quinolinium 3,5-dinitrobenzoate: A novel third order non-linear optical material for optoelectronic applications. Spectrochimica Acta Part a Molecular and Biomolecular Spectroscopy, 249 (2020) 119304. https://doi.org/10.1016/j.saa.2020.119304

[21] GM. Sheldrick, (1997) SHELXS-97, Program for the solution of crystal structures, University of Gottingen, Gottingen, Germany.

[22] GM. Sheldrick, Phase annealing in SHELX-90: direct methods for larger structures. Acta Crystallographica Section A: Foundations of Crystallography, 46, (1990) 467-473. https://doi.org/10.1107/S0108767390000277

[23] T. Portada, D. Margetić, V. Štrukil. Mechanochemical catalytic transfer hydrogenation of aromatic nitro derivatives. Molecules 23, (2018) 3163. https://doi.org/10.3390/molecules23123163

[24] J. Zhu, Z. Yang, Y. Chen, M. Chen, Z. Liu, Y. Cao, J. Zhang, G. Qian, X. Zhou, X. Duan, Mechanistic insights into the active intermediates of 2,6-diaminopyridine dinitration. Chinese Journal of Chemical Engineering, 56, (2022) 160–168. https://doi.org/10.1016/j.cjche.2022.06.024

[25] CS. Karthik, N. Maithra, AHU. Kumar, JR. Rajabathar, KP. Sukrutha, MK Hema, NK. Lokanath, Exploration of one-dimensional hydrogen bonding organic framework (1D-HOF) and charge transfer dynamics in N'-benzylbenzohydrazide: A comprehensive structural and quantum computational investigation. Journal of Molecular Structure, 1307 (2024) 137845. https://doi.org/10.1016/j.molstruc.2024.137845

[26] R. Takouachet, R. Benali-Cherif, E-E Bendeif, K. Bouchouit, W. Falek, B. Sahraoui, A. Rahmouni, N. Benali-Cherif, Nonlinear optical properties and structural characterization of a series of carboxyanilinium hydrogen selenite hybrids: Synthesis, first-principles calculations and correlation analysis for advanced photonic applications. Inorganic Chemistry Communications, 170 (2024) 113439. https://doi.org/10.1016/j.inoche.2024.113439

[27] JA Fernández, Exploring hydrogen bond in biological molecules. Journal of the Indian

Institute of Science, 100 (2019) 135–54. https://doi.org/10.1007/s41745-019-00146-4

[28] A. Choperena, P. Painter, Hydrogen Bonding in Polymers: Effect of Temperature on the OH Stretching Bands of Poly(vinylphenol). Macromolecules,42 (2009) 6159–65. https://doi.org/10.1021/ma900928z

[29] AH. Hameed, G. Ravi, R. Dhanasekaran, P. Ramasamy, Studies on organic indole-3-aldehyde single crystals. Journal of Crystal Growth, 212 (2000) 227-232. https://doi.org/10.1016/S0022-0248(99)00896-9

[30] KK. Bamzai, PN. Kotru, BM. Wanklyn, Investigations on indentation induced hardness and fracture mechanism in flux grown DyAlO3 crystals. Applied Surface Science, 133 (1998) 195-204. https://doi.org/10.1016/S0169-4332(98)00187-1

[31] EM. Onitsch, Uber die mikrohärte der metalle. Microscopia, 2 (1947) 131.

[32] M. Hanneman, Metallurgia Manchu, 1941. Manch, 23:135-140.

[33] ZW. Zhang, Z. Li, Y. Liu, JT. Wang, Path dependency of plastic deformation in crystals: work hardening, crystallographic rotation and dislocation structure evolution. Crystals, 12 (2022) 999. https://doi.org/10.3390/cryst12070999

[34] SA. Meguid, Interatomic Bonds and Defects in Solids. In: Atomistic and Continuum Fracture Mechanics of Solids. Springer, Cham., (2024) 119-131. https://doi.org/10.1007/978-3-031-56085-9_5

[35] MI. Bell, Frequency Dependence of Miller's Rule for Nonlinear Susceptibilities. Physical Review B, 6 (1972) 516. https://doi.org/10.1103/PhysRevB.6.516

[36] C. Zhang, X. He, Q. Lu, High-frequency low-dielectric-loss in linear-backbone-structured polyimides with ester groups and ether bonds. Communication Materials, 5, (2024) 55. https://doi.org/10.1038/s43246-024-00502-7

[37] R. Thirumurugan, S. Priyadharshini, B. Babu, BM Babu, K. Anitha, An efficient phase matching second harmonic generation of 2-amino-4-methylpyridinium quinoline-2-carboxylate (C16H15N3O2) organic single crystal: structural, optical, thermal, and computational investigations. Journal of Molecular Structure, (2025) 141453. https://doi.org/10.1016/j.molstruc.2025.141453

[38] M. Miar, A. Shiroudi, K. Pourshamsian, AR. Oliaey, F. Hatamjafari, Theoretical investigations on the HOMO–LUMO gap and global reactivity descriptor studies, natural bond orbital, and nucleus-independent chemical shifts analyses of 3-phenylbenzo[d]thiazole-2(3H)-imine and itspara-substituted derivatives: Solvent and substituent effects. Journal of Chemical Research, 45 (2020) 147–158. https://doi.org/10.1177/1747519820932091

[39] P. Senet, Chemical hardnesses of atoms and molecules from frontier orbitals. Chemical Physics Letters, 275 (1997) 527–532. https://doi.org/10.1016/s0009-2614(97)00799-9

[40] H. Tandon, T. Chakraborty, V. Suhag, A New Scale of the Electrophilicity Index Invoking the Force Concept and Its Application in Computing the Internuclear Bond Distance. Journal of Structural Chemistry, 60, (2019) 1725–1734. https://doi.org/10.1134/S0022476619110040

[41] RG. Parr, W. Yang, Density functional approach to the frontier-electron theory of chemical reactivity. Journal of the American Chemical Society, 106, (1984) 4049–4050. https://doi.org/10.1021/ja00326a036

[42] DA. Kleinman, Nonlinear dielectric polarization in optical media. Physical Review, 126, (1962) 1977–1979. https://doi.org/10.1103/physrev.126.1977

[43] N. Elleuch, W. Amamou, AB. Ahmed, Y Abid, H Feki, Vibrational spectroscopic study, charge transfer interaction and nonlinear optical properties of l-asparaginium picrate: A density functional theoretical approach. Spectrochimica Acta Part a Molecular and Biomolecular Spectroscopy, 128, (2014) 781–789. https://doi.org/10.1016/j.saa.2014.02.159

[44] M. Sheik-Bahae, AA. Said, EW. Van Stryland, High-sensitivity, single-beam n_2 measurements, Optics Letters, 14, (1989) 955. https://doi.org/10.1364/ol.14.000955

[45] M. Sheik-Bahae, AA. Said, TH. Wei, DJ. Hagan, EW. Van Stryland, Sensitive measurement of optical nonlinearities using single beam. IEEE Journal of Quantum Electronics, 26, (1990) 760-769. https://doi.org/10.1109/3.53394

[46] G. Siva, R. Bharathikannan, B. Mohanbabu, Synthesis, characterization and biological studies of a new adduct single crystal of hexamethylenetetramine:benzilic acid. Materials Today Proceedings, 33 (2020) 4171–6. https://doi.org/10.1016/j.matpr.2020.07.058

Authors Contribution Statement

P. Rohini: Writing, Review & Editing; G. Siva: Methodology, Data collection, Analysis, Writing & Originaldraft; R. Bharathikannan: Conceptualization, Supervision, Validation, Writing, Review & Editing; All authors read and approved the final manuscript.

Funding

The authors declare that no funds, grants or any other support were received during the preparation of this manuscript.

Competing Interests

The authors declare that there are no conflicts of interest regarding the publication of this manuscript.

Data Availability

The data supporting the findings of this study can be obtained from the corresponding author upon reasonable request.

Has this article screened for similarity?

Yes

About the License